Journal of Materials Chemistry B

Accepted Manuscript

This article can be cited before page numbers have been issued, to do this please use: L. He, S. Ji, H. Lai and T. Chen, *J. Mater. Chem. B*, 2015, DOI: 10.1039/C5TB01501D.

ROYAL SOCIETY OF CHEMISTRY

www.rsc.org/materialsB

Cite this: DOI: 10.1039/c0xx00000x

www.rsc.org/xxxxxx

View Article Online
DOI: 10.1039/C5TB01501D

ARTICLE TYPE

Selenadiazole Derivatives as Theranostic Agents for Simultaneous Cancer Chemo-/Radiotherapy by Targeting Thioredoxin Reductase

Lizhen He, Shengbin Ji, Haoqiang Lai, Tianfeng Chen*

Received (in XXX, XXX) Xth XXXXXXXXX 20XX, Accepted Xth XXXXXXXXX 20XX
DOI: 10.1039/b000000x

The lack of early and timely diagnosis of tumors and the monitoring of their response to therapeutics have limited the successful cancer treatments. Theranostic agents are expected to realize the dual-purpose of simultaneous diagnosis and therapy for treatments of cancers. In the present study, we have examined the effects of chemical structure of selenadiazole derivatives (SeDs) on their anticancer efficacy and radio-sensitization against clinically used X-ray. The results showed that, the introduction of nitro group (-NO_2) into SeD-**3** significantly enhanced the anticancer activity of SeDs. The higher lipophilicity endowed SeD-**3** higher cellular internolization ability, resulting in higher cellular uptake and anticancer efficacy. Specifically, the capacity of autofluorescence allowed the use of SeD-**3** as a promising theranostic agent to directly monitor the cellular uptake, localization and biodistribution *in vitro* and *in vivo*. Interestingly, SeD-**3** also significantly enhanced the sensitivity of HeLa cervical cells to X-ray-induced apoptosis by targeting inhibition of TrxR and promoting intracellular ROS overproduction, which activated the downstream ROS-mediated signaling pathways to regulate cell apoptosis. Furthermore, SeD-**3** exhibited satisfactory *in vivo* antitumor efficacy through inhibition of tumor proliferation and induction of tumor cell apoptosis, and showed no toxicity to the main organs. Moreover, from the results of hematological analysis, we found that, not only inhibiting the tumor growth, treatment of SeD-**3** also alleviated the damage of liver, kidney and heart function of nude mice induced by HeLa xenografts. Taken together, this study demonstrates that, SeDs could be further developed as effective and safe theranostic agent for simultaneous cancer chemo-/radiotherapy.

1 Introduction

Although the currently used chemotherapeutic drugs face serious side effects, including nephrotoxicity, neurotoxicity, neutropenia, thrombocytopenia and anemia, chemotherapy is still an important and effective treatment method for cancers.[1-3] However, the lack of early and timely diagnosis of tumors and the monitoring of their response to therapeutics have limited the successful cancer treatments. Theranostic agents are expected to realize the dual-purpose of simultaneous diagnosis and therapy in for treatments of cancers treatment.[4-8] Recently, substantial studies have reported the use of nanomaterials as theranostic agents in combination with imaging methods, including computed tomography (CT), positron emission tomography (PET) and magnetic resonance imaging (MRI).[9-13] For example, *Ke et al.* have constructed gold nanoshelled liquid perfluorocarbon magnetic nanocapsules for nanotheranostic platform to enhance the bimodal ultrasound and magnetic resonance imaging, meanwhile serve as efficient photoabsorbers for NIR photothermal tumor ablation.[14] *Zhang et al.* also reported a kind of activatable hyaluronic acid nanoparticles as a theranostic agent for optical/photoacoustic image-guided photothermal therapy for malignant cancer.[15] Recently, small molecular complexes were also developed as theranostic agent in cancer therapy, especially the metal complex.[16-19] Comparing with nanodrug system, small molecules were promising to be theranostic agent owing to their straightforward synthesis, capacity of autofluorescence and easy internalization in cells. For instance, *Yuan et al.* have developed targeted platinum (Ⅳ) prodrug as a theranostic agent that could monitor the therapeutic response and induce the cell apoptosis in tumor situ.[6] However, the clear elucidation of the anticancer mechanisms of the theranostic metal complex remains critical challenge for their clinical development, and thus need further elaboration. Therefore, it is of great significance to construct new theranostic agents with high activity and low toxicity.

Radiotherapy is a crucial primary treatment in clinical cancer therapy, which uses high-energy X-ray or γ-ray to kill cancer cells by creating excess ROS.[20-22] However, X-ray or γ-ray radiation therapy still faced the challenges of no selectivity between cancer and normal cells, and radioresistance of some hypoxic tumors. Therefore, it is of great significance to utilize the

high-efficiency and low-toxicity radiosensitizers to reduce the dose of radiation and enhance the sensitivity to tumor cells. Selenium (Se) has been well documented as excellent trace elements for humans and animals owing to their extensive pharmacological actions, important physiological functions and the necessary components of Se-dependent enzymes.[23-26] In the past decades, substantial researches have reported the promising anticancer activity of Se-containing species, including organic selenocompounds, inorganic Se and Se nanoparticles.[27-32] Among them, selenadiazole derivatives (SeDs) as typical organic selenium compounds have aroused great interest about their properties of anticancer activity by researchers.[33-35] For instance, benzo[c][1,2,5]selenadiazole and 5-methylbenzo[c][1,2,5] selenadiazole have been used as control compounds to compare the anticancer activities of newly synthesized SeDs in some cancer cell lines, [36, 37] but their activities were not potent enough. For 5-nitrobenzo[c][1,2,5] selenadiazole, although previous studies have demonstrated its pesticidal activities,[38] little information about the anticancer activity, action mechanisms and radiosensitization effects of these SeDs is available. Recently, we have found that, the organic selenocompounds, selenoamino acid and selenium nanoparticles have potential radiosensitivity.[39, 40] Our previous studies also showed that, selenadiazole derivatives acted as radiosensitizers of X-ray through inhibition of thioredoxin reductase (TrxR) activity.[35] However, the action mechanisms remain elusive. Interestingly, studies also found that Se exhibited a significant reduction in toxicity of chemotherapy and radiotherapy, but without compromising their effectiveness durign treatments.[41] Therefore, the search for more effective, safe and novel SeDs to antagonize cancer radioresistance have kindled our great interest of scientists.

TrxR is a homodimeric selenoenzyme which plays an important role in some crucial physiological functions, including antioxidant defensive system, redox-regulated signaling pathways and cell proliferation.[42-44] Studies have found that TrxR was highly expressed in cancer cells, which can activate the oxidized thioredoxin (Trx) to regulate intracellular redox balance through counteracting excess reactive oxygen species (ROS).[45-47] Recent studies have suggested TrxR as pharmacological target for metal complexes during cancer treatment.[48-52] For example, *Che et al.* have developed a binuclear gold (Ⅰ) complex utilizing the mixed bridging of bis(N-heterocyclic carbene) ligands to act as TrxR inhibitor for anticancer and antiangiogenesis *in vivo*.[49] Selenocysteine, plays an important role in the constituent part of some redox enzymes, including TrxR and glutathione peroxidase. Thereupon, organic selenocompounds would be effective TrxR inhibitor in cancer therapy. In the present study, we have synthesized a series of SeDs by facile method, and elucidated the effects of chemical structure on their anticancer efficacy and radio-sensitization against clinically used X-ray. The results showed that, the introduction of nitro group (-NO_2) into SeD-**3** significantly enhanced the anticancer activity of SeDs. The autofluorescence property allowed the use of SeD-**3** as a promising theranostic agent to directly monitor the cellular uptake, localization and biodistribution *in vitro* and *in vivo*. Interestingly, SeD-**3** also significantly enhanced the sensitivity of HeLa cervical cells to X-ray-induced apoptosis by targeting inhibition of TrxR and promoting intracellular ROS overproduction, which activated the downstream ROS-mediated signaling pathways to regulate cell apoptosis. Furthermore, SeD-**3** exhibited satisfactory *in vivo* antitumor efficacy through inhibition of tumor proliferation and induction of tumor cell apoptosis, and showed no toxicity to the main organs. Taken together, this study demonstrates that, SeDs could be further developed as effective and safe theranostic agent for cancer chemo-/radiotherapy.

2 Experimental sections

Synthesis and characterization of SeDs (1-3)

SeDs (**1-3**) were synthesized according to previous methods with modifications.[35, 39, 53] Briefly, 10 mmol corresponding 3, 4-diaminobenzene dissolved in 350 ml hydrochloric acid solution (HCl: H_2O = 1:5) in a 1000 ml flask. 10 mmol SeO_2 which dissolved in 50 ml hot distilled water added into the flask drop by drop through a constant pressure funnel, and then stirred for 2 h. After the reaction completed, sodium hydroxide solution was used to change the pH to about 7.0, filtered, got the rude products. The pure target compounds were further isolated by recrystallization. Yield: 65%-70%. The obtained SeDs (**1-3**) were characterized with ESI-MS, ^{1}H NMR, ^{13}C NMR, UV–vis and fluorescence spectroscopy.

SeD-1. The compound was prepared according to general procedure. ESI-MS (in $CHCl_3$): *m/z* calcd for $C_6H_4N_2Se$ $(M+H)^+$ 183.9; found 185.2. ^{1}H NMR (500 MHz, DMSO, δ, ppm): 7.91 – 7.79 (m, 1H), 7.65 – 7.49 (m, 1H). ^{13}C NMR (125 MHz, DMSO, δ, ppm): 160.2, 129.7, 123.7.

SeD-2. The compound was prepared according to general procedure. ESI-MS (in $CHCl_3$): *m/z* calcd for $C_7H_6N_2Se$ $(M+H)^+$ 197.9; found 199.2. ^{1}H NMR (500 MHz, DMSO, δ, ppm): 7.74 (d, *J* = 9.1 Hz, 1H), 7.65–7.58 (m, 1H), 7.41 (dd, *J* = 9.1, 1.7 Hz, 1H), 2.43 (d, *J* = 1.1 Hz, 3H). ^{13}C NMR (125 MHz, DMSO, δ, ppm): 160.7, 159.2, 140.2, 133.1, 122.9, 121.5, 21.6.

SeD-3. The compound was prepared according to general procedure. ESI-MS (in $CHCl_3$): *m/z* calcd for $C_6H_3N_3O_2Se$ $(M-H)^+$ 228.9; found 227.2; ^{1}H NMR (500 MHz, DMSO, δ, ppm): 8.83 (d, *J* = 2.3 Hz, 1H), 8.25 (dd, *J* = 9.7, 2.3 Hz, 1H), 8.09 (d, *J* = 9.7 Hz, 1H). ^{13}C NMR (125 MHz, DMSO, δ, ppm): 160.5, 157.7, 147.9, 124.0, 121.81, 119.68.

Cell culture and MTT assay

Human cancer cell lines used in this study were purchased from American Type Culture Collection, and the normal human liver cell line (L02) was obtained from Nanjing KeyGEN Biotech. All the cells were incubated with DMEM medium which contain 10% of the fetal bovine serum, 100 units/ml of the penicillin and 50 units/ml of the streptomycin at 37 ℃in humidified incubator with 5% CO_2 atmosphere. Cell viability induced by SeDs (**1-3**) and X-ray for 72 h was analysed by MTT assay.[28]

Determination of TrxR inhibition

HeLa cellular proteins were extracted with cell lysis and conducted the BCA assay to examine the concentrations. The inhibition of TrxR in HeLa cells induced by SeDs (**1-3**) at different concentration within 1 h was determined by thioredoxin reductase assay kit (Cayman) as the method of manufacturer's instructions.[45, 54]

View Article Online
DOI: 10.1039/C5TB01501D

Binding studies between SeDs (1-3) and TrxR model peptide

1 mg/ml of the SeDs (**1-3**) was added in to TrxR model peptide (AGUVGAGLIK) solution with the ratio of 1:1 and incubated for 24 h, respectively. Then MALDI-TOF-MS assay was carried out to determine the interaction between SeDs (**1-3**) and TrxR model peptide.[55, 56]

Measurement of SeDs (1-3) lipophilicity

The lipophilicity of SeDs (**1-3**) was determined by the "shake-flask" method as previously reported.[57] The lipo-hydro partition coefficient was determined by the ratio of the contents of SeDs in oil and aqueous phases, and the *logP* was calculated as the logarithm of the ratio.

Cellular uptake and localization of SeDs (1-3)

HeLa cells (8×10^4 cells/ml, 2 ml) were seeded in confocal glass dishes and allowed to adhere for 24 h. The cells were then incubated with SeDs (**1-3**) at 15 μM for 4 or 12 h, respectively. The treated cell nucleus were labeled with 1 ug/ml of hoechst and determined the cellular uptake and localization of SeDs (**1-3**) with confocal fluorescence microscope (LSM 510 META).

Clonogenic assays

HeLa cells (1×10^3 cells/ml, 2 ml) were seeded in 6-well plates and allowed to adhere for 24 h. The cells were then incubated with SeD-**3** for 4 h and then irradiated with X-ray (2 Gy). After 8-days incubation, the cells were stained with 0.5% of the crystal violet, and evaluated the survival fraction of the clones.

Determination of TrxR inhibition induced by SeDs and X-ray

HeLa cellular proteins treated with or without SeDs (**1-3**) and X-ray (2 Gy) for 24 h were extracted with cell lysis and conducted the BCA assay to examine the concentrations. The inhibition of TrxR in HeLa cells induced by SeDs (**1-3**) and X-ray was determined by thioredoxin reductase assay kit (Cayman). The clinical X-ray radiation was carried out with Elekta Precise linear accelerator.

Measurement of intracellular ROS generation

Briefly, HeLa cells (1×10^5 cells/ml, 0.1 ml) were seeded in 96-well plates and allowed to adhere for 24 h. The cells were then incubated with SeD-**3** for 4 h and irradiated with X-ray (2 Gy). After stained with DCF-DA for another 20 min, the cells were measured with fluorescence microplate reader (Tecan SAFIRE). The intracellular ROS generation was evaluated with the increase of fluorescence value and expressed as the percentage of control.

Flow Cytometric Analysis

HeLa cells (2×10^4 cells/ml, 6 ml) were treated with different concentrations of SeD-**3** for 4 h and then irradiated with or without X-ray (2 Gy). After incubation for another 24 h, the cells were collected and stained with PI, and analyzed the cell cycle distribution by flowcytometer (Beckman Coulter).[29 58]

TUNEL- Hoechst co-staining assay

HeLa cells (8×10^4 cells/ml, 2 ml) were seeded in confocal glass dishes and allowed to adhere for 24 h. The cells were incubated with 2 μM of SeD-**3** for 4 h and then irradiated with or without X-ray (2 Gy). After incubation for another 24 h, the cells were then fixed and conducted with TUNEL- Hoechst co-staining assay experiments to determine the cell apoptotic characteristic as the literature reported methods.[59]

Determination of caspase-3 activity

HeLa cellular proteins treated with or without 2 μM of SeD-**3** and X-ray (2 Gy) for 24 h were extracted with cell lysis and conducted the BCA assay to examine the concentrations. Caspase-3 activity in HeLa cellular proteins was determined using caspase activity kit (BD Biosciences).[59]

Western blot analysis

The expression levels of proteins associated with different signaling pathways in HeLa cells induced by SeD-**3** and X-ray for 24 h were determined by western blot analysis.[60, 61]

***In vivo* fluorescence imaging**

The HeLa xenografts nude mice were intravenously injected with 2 mg/kg of SeD-**3**, then anesthetized and monitored with fluorescence imaging system (Night OWL II LB 983) at different time points (0, 6, 12, 24, 48 and 72 h). After 24 and 72 h, the brain, heart, liver, spleen, lungs, kidney and tumor of each group were taken out and determined the biodistribution of SeD-**3** in the main organs with fluorescence imaging technique, after then the Se concentration was determined by ICP-AES.[62]

***In vivo* antitumor activity**

The HeLa xenografts nude mice (n=6) were intravenously injected with 2 mg/kg of SeD-**3** every other day for 15 times, and detected the maximal length (*l*) and width (*w*) of tumor and the body weight every day. After administration with SeD-**3**, the tumor was striped and weighed. The tumor volume was obtained as the formula: volume = $l\times w^2/2$. The sections of tumor and main organs were conducted the H&E staining to observe pathological changes caused by SeD-**3**. The tumor sections were conducted immunohistochemical (IHC) assay to examine the expression of proteins which associated with the inhibition of tumor growth. We collected the venous blood samples from the nude mice eye before kill them, and centrifuged to obtain plasma. Then we conducted the hematology analysis to determine the function of liver, kidney and heart. All the animal experiments were authorized according to Animal Experimentation Ethics Committee of Jinan University.

Statistical analysis

All experiments were carried out at least in triplicate and results were expressed as mean ±S.D. The statistical software package (SPSS Inc., Chicago, IL) was used for statistical analysis. Statistically significant between two groups was analyzed using the $P<0.05$ or $P<0.01$ (**). Bars with different characters are statistically different at $P<0.05$ level.

3 Results and Discussion

Synthesis and *in vitro* anticancer activities of SeDs (1-3)

In the present study, a series of SeDs has been synthesized by facile method, and their anticancer and radio-sensitization activities were also examined. The chemical structure of the SeDs, namely, benzo[c][1,2,5]selenadiazole (SeD-**1**), 5-

Table 1. Cytotoxic effects of SeDs (**1-3**) on human cancer and normal cells.

Complex	IC_{50}[a]						EC_{50}[c]	
	HeLa	Siha	Caski	HepG 2	A549	L02[b]	HeLa	*logP*[d]
SeD-**1**	>400	>400	73.0	86.2	197.1	121.7	>400	-6.26
SeD-**2**	>400	>400	91.2	115.8	>400	130.3	>400	-3.83
SeD-**3**	4.8	5.5	3.8	2.9	5.0	18.0	18.7	2.14
Cisplatin	11.8	17.0	10.6	13.6	16.9	10.3	--	--

a: Concentration for 50% cell growth inhibition.

b: Normal cells.

c: Concentration for 50% TrxR inhibition effect.

d: Lipo-hydro partition coefficient.

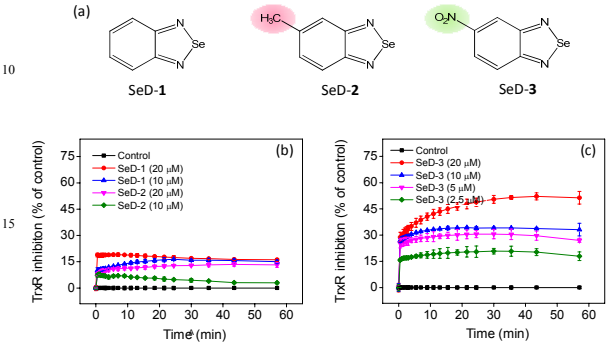

Figure 1. (a) Chemical structure of the SeDs (**1-3**). (b, c) Inhibition of SeDs (**1-3**) on intracellular TrxR activity in HeLa cells.

methylbenzo[c][1,2,5]selenadiazole (SeD-**2**) and 5-nitrobenzo[c][1,2,5]selenadiazole (SeD-**3**), were demonstrated in **Scheme S1**, and characterized by ESI-MS, ^{1}H NMR and ^{13}C NMR. Then we examined the cytotoxic effects of SeDs (**1-3**) against human cancer and normal cells by MTT assay. As shown in **Table 1**, SeD-**1** and SeD-**2** demonstrated low cytotoxicity toward the tested cancer cells, including cervical cancer cells (HeLa, Siha, Caski), hepatocellular carcinoma cells (HepG2) and lung carcinoma cells (A549). In contrast, SeD-**3** exhibited strong and broad-spectrum anticancer activity. Comparing with the positive control of cisplatin, SeD-**3** exhibited higher anticancer activity and lower cytotoxicity to normal cells. For instance, the IC_{50} value of SeD-**3** toward HeLa cells was 4.8 μM, which was significantly lower than that of cisplatin (11.8 μM). While the IC_{50} value of SeD-**3** and cisplatin towards L02 human normal cells was 18.0 μM and 10.3 μM, respectively. The safety index (IC_{50} (L02) / IC_{50} (HeLa)) of SeD-**3** was 3.75, which was significantly higher than those of cisplatin (0.87). These results indicate that SeD-**3** exhibits higher anticancer efficacy and safety index than SeD-**1**, SeD-**2** and cisplatin. The lipophilicity of complex is closely related to the cytotoxicity. Then we examined the lipophilicity (lipo-hydro partition coefficient, *log P*) of SeDs to confirm this hypothesis. As shown in **Table 1**, the *log P* of SeD-**3** was about 2.14, which was much higher than that of SeD-**1** (-6.26) and SeD-**2** (-3.83).

SeDs (1-3) inhibit HeLa cell growth by targeting TrxR

Intracellular TrxR system plays an important role in maintaining redox balance through counteracting excess ROS, making it as a promising pharmacological target for anticancer agents during

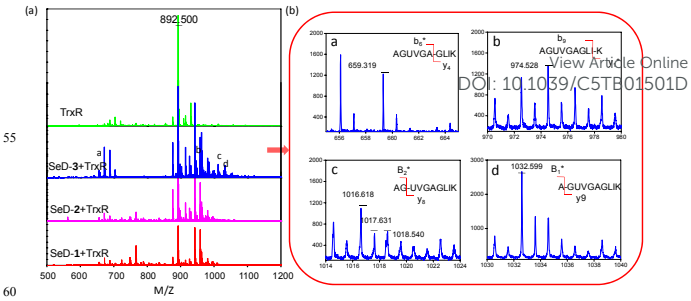

Figure 2. Interaction of SeDs (**1-3**) with TrxR peptide. MALDI-TOF-MS spectrum of the free TrxR and SeDs (1 mg/ml) after incubation with TrxR peptide for 24 h. The amino acids marked with asterisk (*) stand for dissected fragments of TrxR.

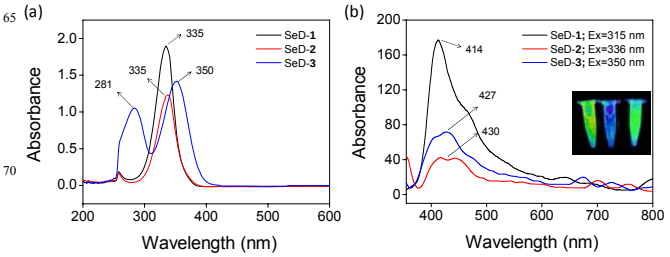

Figure 3. The UV- *vis* spectra (a) and fluorescence spectroscopy (b) of SeDs (**1-3**) at 1mM.

cancer treatment.[45] Therefore, in this study, we have examined the inhibition of TrxR by SeDs (**1-3**) in HeLa cells after treatment for 24 h. As shown in **Table 1**, the EC_{50} (50% TrxR inhibition) value of SeD-**3** was 18.7 μM, while those for SeD-**1** and SeD-**2** were higher than 400 μM, indicating the higher TrxR-inhibitory activities of SeD-**3**. These results were closely related and consistent with the cytotoxic effects of SeDs (**1-3**) to HeLa cells. To further confirm the roles of TrxR in the anticancer action of SeDs, we also examined their inhibitory kinetics on intracellular TrxR in HeLa cell lysates. As shown in **Figure 1**, SeD-**3** significantly inhibited the TrxR activity in dose- and time-dependent manner, which was much higher than those of SeD-**1**and SeD-**2**. Interestingly, SeD-**1** and SeD-**2** inhibited the TrxR activity to 15% at 20 μM within 1 h, which was much differet from their EC_{50} in whole cell model. The difference should be due to the use of different models and different detection methods. In the cell lysate model, SeDs could react with TrxR protein directly, therefore resulting higher inhibition efficacy than that in whole cell model, while in the whole cell model, the cell membrane could affect the drug penetrating and the other intracellular proteins could interfere with the interaction between SeDs and TrxR protein, resulting in low inhibition efficacy.

Based on the strong TrxR-inhibitory activities of SeD-**3** in HeLa cells, we used selenocysteine-containing peptide (AGUVGAGLIK) as the model of TrxR to examine the chemical interactions between SeD-3 and TrxR on the molecular level. MALDI-TOF-MS assay was carried out to determine the binding of the compounds on the active site of TrxR peptide. As shown in **Figure 2a**, after incubation with TrxR peptide for 24 h, some new fragment peaks were detected in the MALDI-TOF-MS spectra of all SeDs, indicating the binding to the compounds to the peptide to form new complexes. For instance, in the spectrum of SeD-**3**, the detection of a new peak at m/z 659.3 was attributed to that the

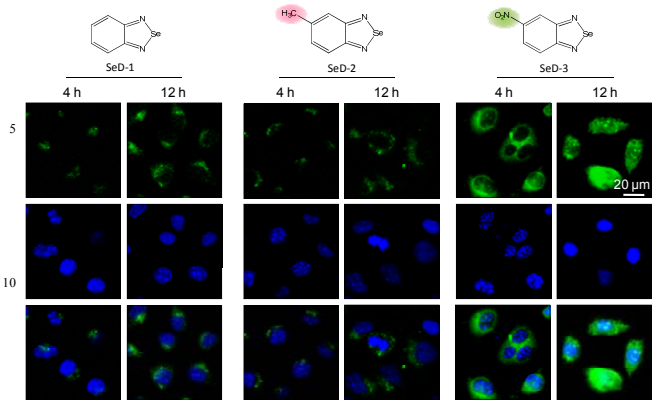

Figure 4. Cellular uptake and localization of SeDs (15 μM) in HeLa cells as examined by confocal imaging.

binding of SeD-**3** the peptide fragment (H-GLIK). The other new molecules at m/z 974.5, 1017.6 and 1032.6 correspond to the banding of SeD-**3** and the peptide fragments of AGUVGAGLI-H, H-UVGAGLIK and H- GUVGAGLIK, respectively (**Figure 2b**). These results indicate that SeDs could target intracellular TrxR by chemical interaction to suppress cancer cell growth.

Cellular uptake, localization and distribution of SeDs (1-3)

From the results of UV–vis and fluorescence spectroscopy, we found that the synthetic SeDs exhibited similar strong absorbance and fluorescence, which could be due to the presence of selenadiazole conjugate plane in their chemical structure (**Figure 3**). In addition, the fluorescence intensity was in the order of SeD-**1** > SeD-**3** > SeD-**2** at the same concentration. The fluorescence of SeD-**1** and SeD-**3** could also be imaged under confocal fluorescence microscope and animal fluorescence imaging system, which allows the applications of SeDs as diagnostic agents during cancer treatment. Based on this property, we next examined the cellular uptake, localization and distribution of SeDs in HeLa cells. As shown in **Figure 4**, after incubated with SeDs (**1-3**) at 15 μM for 4 h, the three compounds were all located in cytoplasm. The fluorescence intensity of SeD-**3** was much stronger than those of SeD-**1** and SeD-**2**, which indicated the higher cellular uptake of SeD-**3** in HeLa cells. After 12 h, we found that SeD-**1** and SeD-**2** was still in cytoplasm, and the fluorescence intensity didn't increased. On the contrary, SeD-**3** entered the cell nucleus and was dispersed over the whole cells, suggesting that SeD-**3** exhibited higher cell membrane permeability. These results may arise from the high *logP* of SeD-**3**. To further confirm the localization of SeDs in HeLa cells, we conducted the quantification analysis of fluorescence intensity to the cell profile after 12-h treatment. As shown in **Figure 5**, the signal intensity of SeD-**1** and SeD-**2** in the cytoplasm of HeLa cells was high at about 1000, but negligible in the nucleus. Nevertheless, we found the high green fluorescence signal (≈2000) exist in the whole HeLa cells, including cytoplasm and nucleus, exposed to SeD-**3**. Further exploration of the changed localization of SeD-**3** in HeLa cells after 4 or 12-h treatment was conducted by three-dimensional (3D) visualization method to scan at increasing depths along the z-axis. As shown in **Figure 6a**, the xy image of 4-h treated cell revealed that the green fluorescence from SeD-**3** only exited in cytoplasm, and there was no discovery

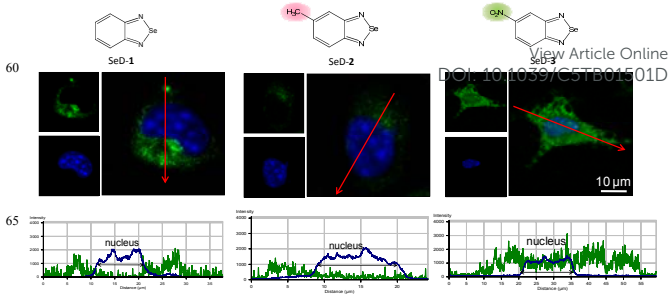

Figure 5. Intracellular localization and distribution of SeDs (15 μM) in HeLa cells after 12-h incubation.

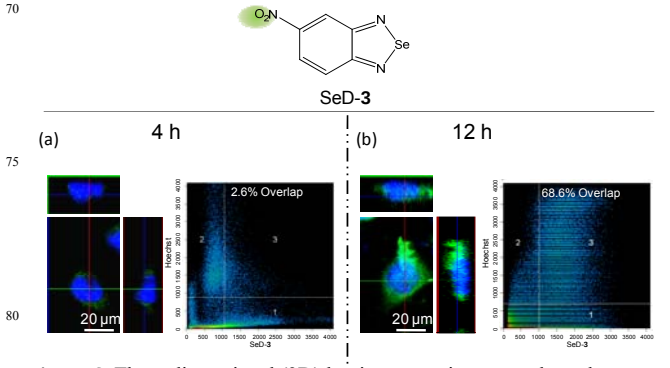

Figure 6. Three-dimensional (3D) luminescence images and overlap rates of HeLa cells after incubated with 15 μM SeD-**3** for 4 h (a) and 12 h (b).

in nuclear regions whether scanning from xz or yz images. The colocalization ratio of green (SeD-**3**) and Hoechst (nuclear) fluorescence was almost 2.6%, further indicating the localization of SeD-**3** only in cytoplasm. Interestingly, as the xy image of 12-h treated cells, we observed the green fluorescence from SeD-**3** filled in the whole cells (**Figure 6b**). The cytoplasm and nuclear regions were also perfectly visualized by strong green fluorescence in xz and yz images. Moreover, the colocalization ratio of the green and blue fluorescence was about 68.6%, suggesting that there was about 31.4% of the SeD-**3** was localized in the cell nucleus, and the other SeD-**3** still existed in the cytoplasm regions. Then we also examined the relative contents of SeD-**3** in the separated nucleus to further confirm the localization of SeD-**3** in HeLa cells after 4-h and 12-h incubation. As shown in **Figure S1**, almost all the SeD-**3** existed in cytoplasm of HeLa cells after 4-h treatment, while there was only very weak fluorescence intensity of SeD-**3** detected in the cell nucleus. However, after 12-h incubation, the fluorescence intensity of SeD-**3** in the nucleus significantly increased. These results clearly demosntrated the translocation of SeD-**3** from cytosol to nucleus, which strengthen and support our results obtained with fluorescent microscopy. Taken together, these results demonstrated that, the slight modification of chemical structure of SeDs effectively alters their cellular uptake and localization. The strong fluorescence of SeDs enables their future application as theranostic agent in cancer therapy.

SeD-3 enhances the radiosensitivity of HeLa cells by targeting TrxR and activating ROS-mediated signaling

Radiotherapy is a crucial primary treatment in clinical cancer

Cite this: DOI: 10.1039/c0xx00000x
www.rsc.org/xxxxxx
View Article Online
DOI: 10.1039/C5TB01501D
ARTICLE TYPE

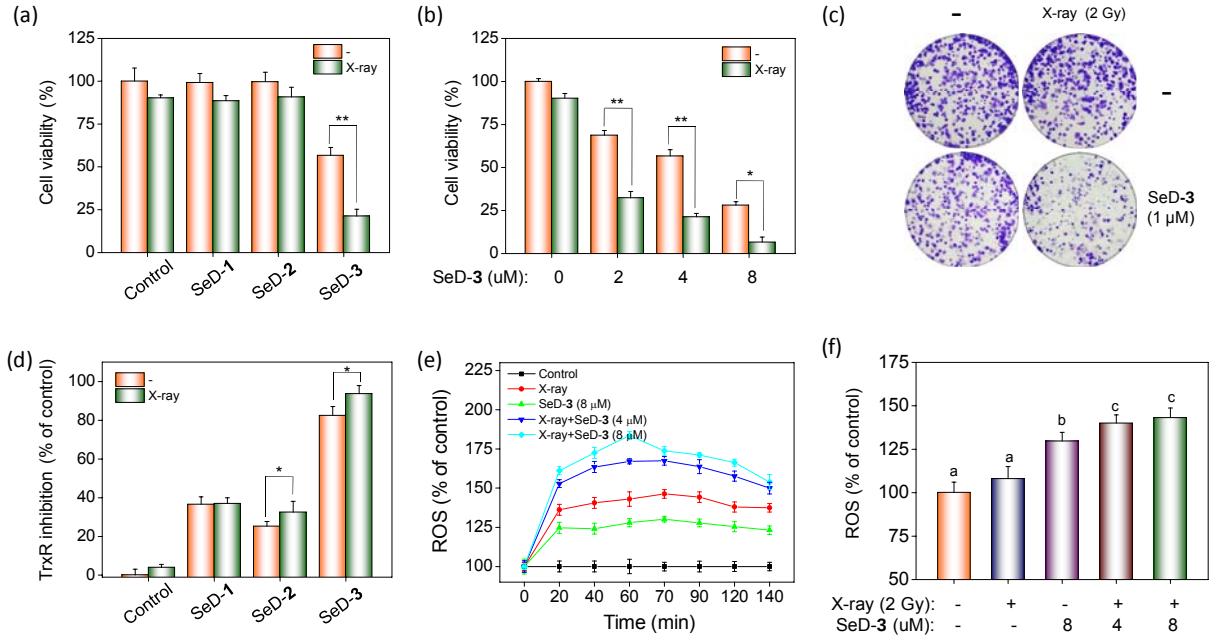

Figure 7. SeD-3 enhances radio-sensitivity of HeLa cells to X-ray by targeting TrxR. (a) Cytotoxic effects of SeDs (**1**-**3**) at 4 μM with or without X-ray on HeLa cells for 24 h. (b) Cell viability of Hela cells treated with different doses of SeD-**3** and X-ray for 24-h incubation. (c) SeD-**3** enhances the inhibitory effects of X-ray on the colony formation of HeLa cells. (d) Inhibition of SeDs (**1**-**3**) at 4 μM and treated with or without X-ray on TrxR activity in HeLa cells for 24 h. Significant difference between treatment and control groups is indicated at * P <0.05, ** P < 0.01 level. (e) Overproduction of ROS in Hela cells treated by SeD-**3** and X-ray. (f) ROS generation in HeLa cells after treated by X-ray and incubated with SeD-**3** for 24 h. Bars with different characters (a, b and c) are statistically different at P < 0.05 level. Values expressed are means ± SD of triplicates.

therapy, which uses high-energy X-ray or γ-ray to kill cancer cells by creating excess ROS. It is of great significance to utilize the high-efficiency and low-toxicity radiosensitizers to reduce the dose of radiation and enhance the sensitivity to tumor cells. The above results have found that SeD-**3** could significantly inhibit the TrxR activity in cancer cells, thus breaking the redox balance, and stop counteracting the excess ROS. Possibly, SeD-**3** could be further developed as an effective radiosensitizers in radiotherapy through regulation of ROS pathway. Therefore, we determined the cell viability of HeLa cells treated by SeDs with the clinical X-ray radiation (2 Gy, the dose of clinical used) to see its radiosensitization effect. As shown in **Figure 7a** and **b**, the X-ray radiation alone only inhibited 10% of HeLa cell growth. Meanwhile, SeD-**1** and SeD-**2** at 4 μM, alone or in combination with X-ray, showed no significant cytotoxicity toward Hela cells. In contrast, 4 μM SeD-**3** significantly enhanced the radiosensitivity of HeLa cells. For instance, the cell viability co-treated with X-ray and SeD-**3** decreased significantly from 56.6% (SeD-**3** treated alone) to 21.2%. Furthermore, we conducted the clonogenic assay to confirm the radiosensitization effects of SeD-**3**. As shown in **Figure 7c** and **Figure S2**, SeD-**3** significantly inhibited the cell colony formation, especially co-treated with X-ray. While the X-ray radiation almost no toxicity to HeLa cells, the survival fraction that treated with 2 Gy of X-ray was about 93%. To further investigate the underlying target accounting to radiosensitivity of SeD-**3**, we examined the TrxR inhibition in HeLa cells treated with 4 μM of the SeDs (**1**-**3**) and X-ray (2 Gy) for 24 h. As shown in **Figure 7d**, the X-ray radiation alone at 2 Gy hardly inhibited the TrxR activity, and the TrxR inhibition triggered by SeD-**1** and SeD-**2** even co-treated with X-ray were about 36.9% and 32.4%, respectively. However, SeD-**3** markedly inhibited the TrxR activity at 93.6% in HeLa cells after co-treated with X-ray. Taken together, these results further suggest that, TrxR could be a potential target for SeD-**3** to enhance the radiosensitivity of HeLa cells.

Intracellular TrxR system plays an important role to counteract the excess ROS to avoid the directly DNA damage in cells. As the inhibition of TrxR, the intracellular redox balance would be broken, thus resulting in intracellular ROS overproduction. To confirm this hypothesis, we conducted the DCF-DA assay to examine the intracellular ROS generation in cells after treated by SeD-**3** and X-ray radiation. As expected, X-ray radiation at 2 Gy triggered amounts of ROS accumulation in HeLa cells, which reached 144.2% at 70 min, higher than the group of 8 μM SeD-**3** alone (130.1%) (**Figure 7e**). Interestingly, as shown in **Figure 7b**, X-ray alone showed no cytotoxicity towards Hela cells at 2 Gy for 24 h, while SeD-**3** at 8 μM inhibited about 72% of HeLa cell growth, which could be due to the different TrxR inhibitory effects of X-ray and SeD-**3**. Briefly, X-ray alone couldn't inhibit TrxR activity, which kept the cells with the ability to scavenge the excess ROS within 24 h, and thus

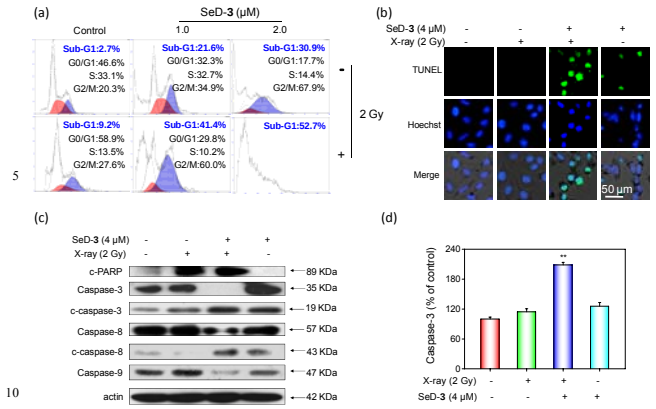

Figure 8. SeD-3 enhances radiation-induced apoptosis of HeLa cells. (a) Flow cytometric analysis of HeLa cells after treated with or without SeD-**3** and X-ray (2 Gy). (b) TUNEL and Hoechst co-staining assay detected the induction of HeLa cell apoptosis induced by SeD-**3** and radiation. (c) Expression levels of the caspase families after treated by SeD-**3** and X-ray. (d) Analysis of caspase-3 activity in HeLa cells treated with SeD-**3** and X-ray for 24 h. Significant difference between treatment and control groups is indicated at * P <0.05, ** P < 0.01 level.

keeping the cells alive. On the contrary, SeD-**3** significantly inhibited the TrxR activity, which impeded the elimination of the excess ROS, finally resulting in cell death. To test and verify this hypothesis, we examined the intracellular ROS generation after treated by X-ray and incubated with SeD-**3** for a long time (24 h). As shown in **Figure 7f**, after 24 h, the ROS generation was declined to 108% in HeLa cells treated by X-ray, while the ROS level in SeD-**3**-treated cells still maintained at high level of 129.6%. Furthermore, ROS generation in HeLa cells after co-treated with SeD-**3** at 8 μM and X-ray was significantly increased to 180% at 60 min, and still maintained at 143% after 24 h. Therefore, the combination of SeD-**3** and X-ray inhibit the TrxR activity, resulting in higher level and longer time of ROS accumulation in HeLa cells to trigger cell death.

Apoptotic cell death induced by SeD-3 and X-ray

Apoptosis and cell cycle arrest are the important potential mechanisms which lead to the inhibition of cell proliferation.[63] In this study, we have conducted flow cytometric analysis to investigate the action mechanism for the radiosensitization of SeD-**3** to X-ray in HeLa cells. As shown in **Figure 8a**, the representative DNA histograms demonstrated that SeD-**3** alone significantly caused both apoptosis and G2/M arrest in HeLa cells in a dose-dependent manner. 2 Gy X-ray also induced slight apoptosis and G2/M arrest. Interestingly, the combination of SeD-**3** with X-ray effectively enhanced the cell apoptosis and cell cycle arrest. For instance, the Sub-G1 peak of HeLa cells treated by 1.0 μM SeD-**3** was about 21.6%, while after co-treatment with X-ray, SeD-**3** induced about 41.4% cells apoptosis at the same concentration. The induction of cell apoptosis induced by SeD-**3** and radiation was further confirmed by TUNEL and Hoechst co-staining assay, which can reflect the DNA fragmentation in apoptotic cells before morphological changes. As shown in **Figure 8b**, the cells treated by X-ray didn't exhibit any apoptotic features, and SeD-**3** also induced a weak apoptosis in HeLa cells. However, after co-treated with SeD-**3** and X-ray radiation, the

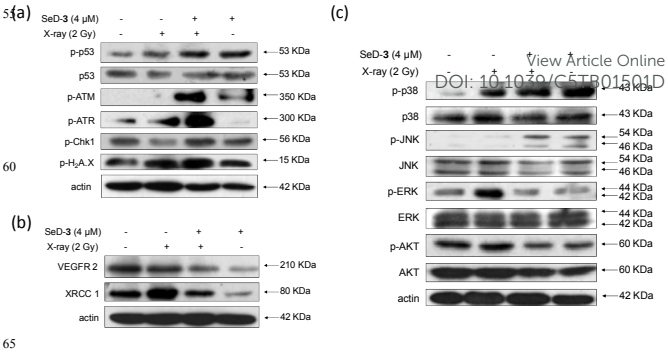

Figure 9. (a) SeD-**3** enhances radiation-induced activation of p53 signaling pathway. (b) SeD-**3** down-regulates the expression of VEGFR2 and XRCC1 in HeLa cells. (c) Effects of X-ray and SeD-**3** on the expression levels of correlative protein of MAPKs and AKT pathways in HeLa cells. Cells were treated with 4 μM SeD-**3** or X-ray for 24 h.

HeLa cells exhibited obviously apoptotic DNA fragmentation, showing a strong green fluorescence in cell nucleus.

Caspase family members are considered as the central regulators in the initiation and execution of cell apoptosis.[63] They could activate the downstream cleavage of PARP that acts as a biochemical marker of cell apoptosis. Thereupon, we conducted the western blot analysis to examine the expression of the relevant protein in HeLa cells apoptosis triggered by SeD-**3** and X-ray radiation. As shown in **Figure 8c**, SeD-**3** caused the activation of caspase-3, caspase-8 and caspase-9 in HeLa cells after co-treated with X-ray, as evidenced by the decrease of the total protein and increase of cleaved caspases expression. The cleavage of PARP was subsequently activated in HeLa cells by the combined treatment. We also examined caspase-3 activity by fluorescence intensity, and found that, it was markedly increased to 208.7% after co-treatment with SeD-**3** and X-ray, which was much higher than that of single treatment (**Figure 8d**). Taken together these results suggest that SeD-**3** effectively enhances the radiosensitivity of HeLa cells to clinically used X-ray by triggering caspases-mediated apoptosis.

ROS downstream signaling pathways triggered by SeD-3 and X-ray

Generally, excess ROS inside the cells could arouse the DNA damage, and activate the downstream ROS-mediated p53 signaling pathway. To demonstrate this hypothesis, we examined the expression level of the relevant protein of DNA damage and p53 in the treated HeLa cells by western blot analysis. As shown in **Figure 9a**, after co-treated with X-ray radiation, SeD-**3** significantly elevated the expression level of p-ATM, p-ATR, p-Chk1 and p-H2A.X, which are the important marker protein of DNA damage. Phosphorylated p53 was subsequently activated in HeLa cells by the combined treatment. We also examined the expression of DNA repair proteins of VEGFR 2 and XRCC 1, the recovery protein of cancer cells after radiation and X-ray repair cross complementing protein. As shown in **Figure 9b**, X-ray radiation triggered the markedly up-regulation of VEGFR 2 and XRCC 1, while SeD-**3** and the co-treatment of SeD-**3** and X-ray could reduce their expression levels, which may be benefit to inhibit the self-repair capabilities of HeLa cells. Furthermore, the MAPK and AKT pathways also play the important roles in the

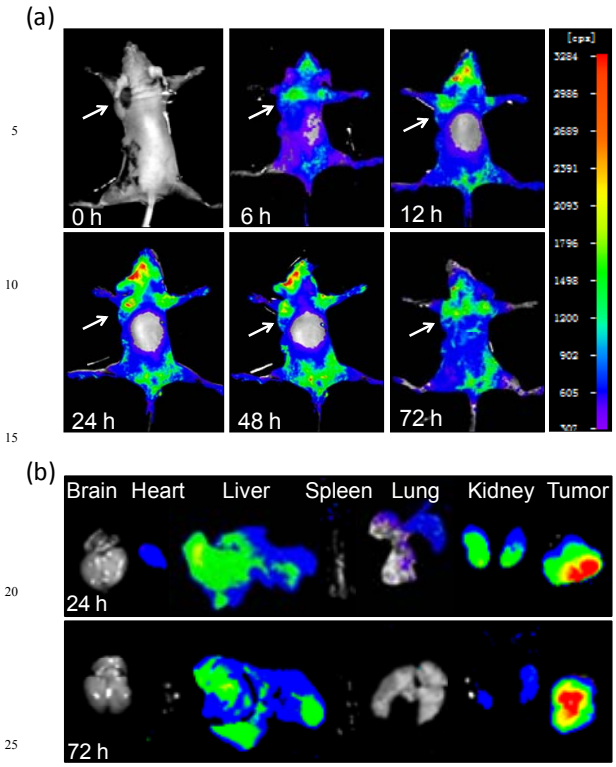

Figure 10. (a) Fluorescence imaging monitors the accumulation and distribution of SeD-**3** (2 mg/kg) in HeLa xenografts nude mice at different time points. (b) The biodistribution of SeD-**3** in the main organs after intravenous injected with SeD-**3** for 24 and 72 h.

process of ROS-induced cell death. It was found that the co-treatment of SeD-**3** and X-ray induced differential phosphorylation of MAPK and AKT relevant protein in Hela cells, including p38, JNK, ERK, and AKT (**Figure 9c**). Taken together these results suggest that, SeD-**3** enhanced the X-ray induced DNA damage and suppressed cell self-repair capability, simultaneously triggered the ROS downstream signaling pathways by SeD-**3** and X-ray.

In vivo theranostic activity of SeD-3

In vivo biodistribution of SeD-**3** in HeLa xenografts nude mice were monitored with animal fluorescence imaging technique at different time points. As shown in **Figure 10a**, SeD-**3** gathered around the tumor site after 12-h intravenous injection and the fluorescence intensity increased after that. A great deal of SeD-**3** was internalized in tumor site at 24 h, and exhibited the long residence time in tumor site. We also determined the biodistribution of SeD-**3** in the main organs, including brain, heart, liver, spleen, lungs, kidney and tumor. From the results of **Figure 10b**, the accumulation of SeD-**3** in tumor was much higher than that in other organs, even after injection for 72 h. SeD-**3** also accumulated in liver and kidney after 24-h injection, but it was decreased after 72 h. To further verify the biodistribution of SeD-**3** in the HeLa xenografts nude mice, we have determined the concentration of Se in the main organs by ICP-AES after 24-h and 72-h intravenous injection. The results showed that the concentration of Se in tumor was much higher than those in other organs (**Figure S3**). Comparing with the 24-h

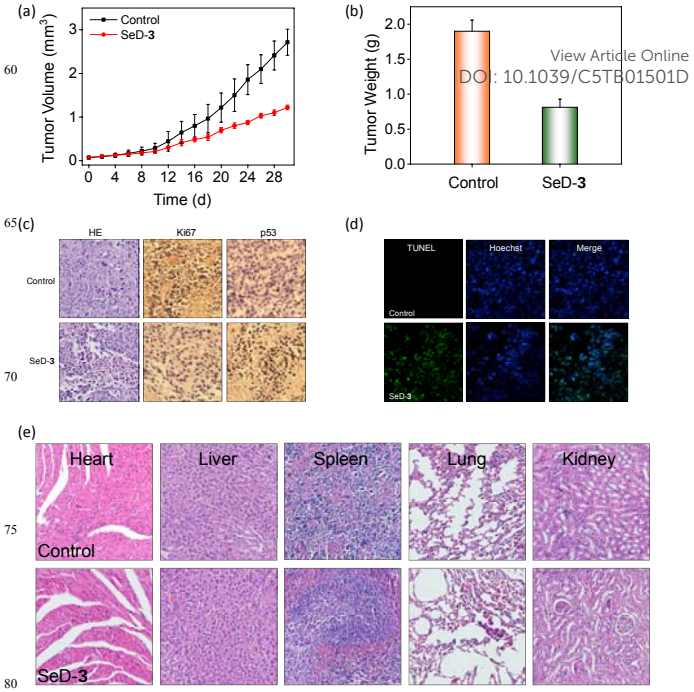

Figure 11. SeD-**3** inhibits tumor growth in vivo. Changes of tumor volume (a) and tumor weight (b) after treated with SeD-**3** at 2 mg/kg for 30 days. (c) H&E staining and in vivo protein expression in tumor xenografts examined by IHC method. (d) TUNEL and Hoechst co-staining assay detected the induction of tumor cell apoptosis induced by SeD-**3**. (e) The toxicity of SeD-**3** on major organs after 30-day treatment.

timepoint, the concentration of Se in the major organs in nude mice treated for 72 h have decreased in different levels. In contrast, the Se content in tumor tissue maintained at high level and increased from 24 to 72 h, which further suggesting the long residence time of SeD-**3** in tumor site and demonstrate the possible *in vivo* cancer-targeting effects of this kind of selenocompounds.

To further examine the *in vivo* anticancer potential of SeD-**3**, we assessed its therapeutic efficacy to the nude mice with HeLa xenografts. As shown in the **Figure 11a** and **b**, after intravenous injection with SeD-**3** at 2 mg/kg for 30 days, both the tumor volume and weight were significantly inhibited comparing with the control. For instance, the tumor volume was decreased from 2.7 mm^3 (the control group) to 1.2 mm^3 after treated by SeD-**3**, and the tumor weight also declined from 1.9 g to 0.81 g, the tumor inhibition rate was high at 57.3%. We simultaneously examined the body weight of the control and treatment groups every day, and found that SeD-**3** didn't inhibit their body growth comparing to the control, indicating the low toxicity of SeD-**3** (**Figure S4**).

Furthermore, we evaluated the *in vivo* antitumor mechanisms of SeD-**3** with immunohistochemical (IHC) assay. As shown in the result of H&E staining (**Figure 11c** and **d**), the control group exhibited typical pathological features of malignancy including mitosis and nuclear abnormalities, while SeD-**3** significantly decreased these features. SeD-**3** also markedly reduced the proliferation of tumor as reflected by the down- regulation of Ki67, and increased the expression level of p53. The results of TUNEL-Hoechst co-staining assay also revealed that, SeD-**3** effectively induced tumor cell apoptosis *in*

Cite this: DOI: 10.1039/c0xx00000x

www.rsc.org/xxxxxx

View Article Online
DOI: 10.1039/C5TB01501D

ARTICLE TYPE

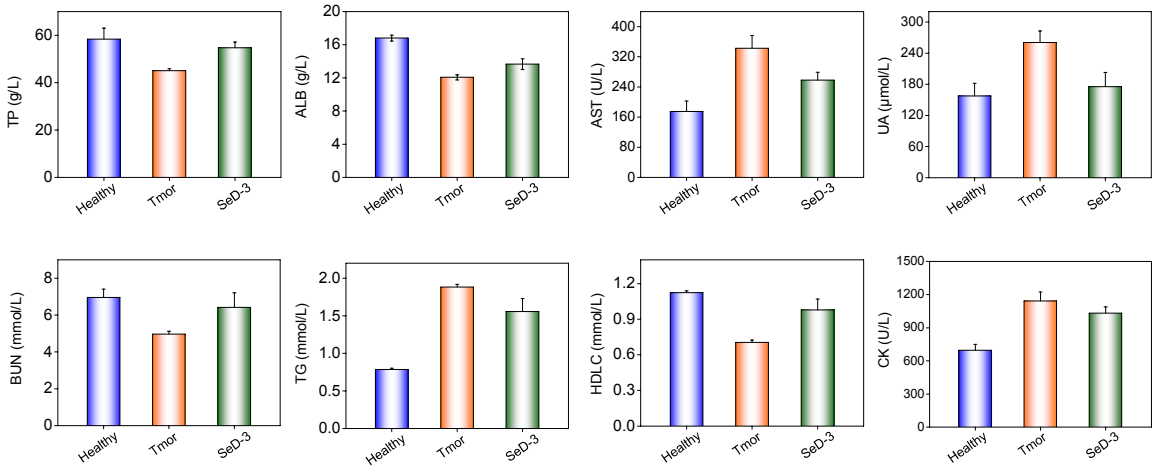

Figure 12. Hematological analysis of healthy and tumor-bearing nude mice, and those treated with SeD-**3** (2 mg/kg) for 30 days. The nude mice in healthy and tumor-bearing groups were treated with saline

vivo. These results indicate that SeD-**3** inhibits tumor growth through activation of p53-mediated apoptosis. In the nude mice model, we also examined the toxic side effects of SeD-**3** to normal tissues. As demonstrated from the results of H&E staining of the main organs, no pathological changes were observed in the heart, liver, spleen, lungs and kidney in nude mice treated with SeD-**3** for 30 days (**Figure 11e**). Then we also conducted the hematology analysis to determine the effects of SeD-**3** on liver and kidney functions of the treated nude mice. As shown in **Figure 12**, comparing with the healthy nude mice (no HeLa xenografts), HeLa xenografts nude mice exhibited obvious acute liver and renal dysfunction, which was reflected by the increase in total protein (TP), albumin (ALB), blood urea nitrogen (BUN) and the decrease of aspartate aminotransferase (AST) and uric acid (UA), which indicate the serious damage of tumor-bearing to the health of nude mice. The damage of liver and kidney also led to the decrease of triglycerides (TG), creatine kinase (CK) and the increase of high-density lipoprotein (HDL-C). Interestingly, not only inhibiting the tumor growth, treatment of SeD-**3** also alleviated the damage of liver, kidney and heart function of nude mice induced by HeLa xenografts, as reflected by the changes in the blood biochemical values toward the normal group. Consistently, we also examined the acute toxicity of SeD-**3**, and found that the half lethal dose (LD_{50}) of SeD-**3** to mice was at about 37.0 ± 2.9 mg/kg body weight. Then we also examined the toxicity of SeD-**3** to normal tissues with histological analysis. As shown in **Figure S5**, SeD-**3** did not show obvious toxicity to the organs at high dose of 20 mg/kg, only a small number of megakaryocytes were observed in spleen, but the slight damage could not hinder the future application of SeD-**3**. Taken together, this study further demonstrated that SeD-**3** acted as an effective and safe theranostic agent for cancer chemo-/radiotherapy *in vitro* and *in vivo*.

4 Conclusions

In summary, herein we have identified SeDs as promising theranostic agents to achieve synergistic chemo-/radiotherapy in cancer cells. The results showed that, the higher lipophilicity endowed SeD-**3** higher cellular internalization in HeLa cells, thus resulting the much higher anticancer activity than SeD-**1** and SeD-**2**. Simultaneously, SeD-**3** also acts as a promising theranostic agent to directly monitor the cellular uptake, localization and biodistribution *in vitro* and *in vivo* because of its capacity of autofluorescence. SeD-**3** also significantly enhanced the sensitivity of HeLa cervical cells to X-ray through inhibition of TrxR and triggering intracellular ROS overproduction, which activated the downstream ROS-mediated signaling pathways to regulate HeLa cells apoptosis. Furthermore, SeD-**3** exhibit satisfactory *in vivo* antitumor efficacy and showed low toxicity, demonstrating its application as theranostic agent for simultaneous cancer chemo-/radiotherapy. Therefore, this study provides useful information for further development of effective and safe theranostic agents for simultaneous cancer chemo-/radiotherapy.

Acknowledgements

This work was supported by National High Technology Research and Development Program of China (863 Program, SS2014AA020538), Science Foundation for Distinguished Young Scholars (S2013050014667) of Guangdong Province, Natural Science Foundation of China, Foundation for High-level Talents in Higher Education of Guangdong, YangFan Innovative & Entepreneurial Research Team Project (201312H05), Guangdong Special Support Program and Guangdong Frontier and Key Technological Innovation Special Funds.

Notes and references

Department of Chemistry, Jinan University, Guangzhou 510632, China. Tel: +86 20-85225962;E-mail: tchentf@jnu.edu.cn.

† Electronic Supplementary Information (ESI) available: [details of any supplementary information available should be included here]. See DOI: 10.1039/b000000x/

View Article Online DOI: 10.1039/C5TB01501D

Reference

1. M. Markman, *Expert Opin. Drug Saf.*, 2003, **2**, 597-607.
2. M. Markman, *Expert Opin. Drug Saf.*, 2003, **2**, 141-146.
3. P. C. Bruijnincx and P. J. Sadler, *Curr. Opin. Chem. Biol.*, 2008, **12**, 197-206.
4. E. K. Lim, T. Kim, S. Paik, S. Haam, Y. M. Huh and K. Lee, *Chem. Rev.*, 2015, **115**, 327-394.
5. F. M. Kievit and M. Zhang, *Adv. Mater.*, 2011, **23**, H217-247.
6. Y. Yuan, R. T. Kwok, B. Z. Tang and B. Liu, *J. Am. Chem. Soc.*, 2014, **136**, 2546-2554.
7. J. K. Rhee, O. K. Park, A. Lee, D. H. Yang and K. Park, *Mar. Drugs*, 2014, **12**, 6038-6057.
8. W. P. Fan, B. Shen, W. B. Bu, X. P. Zheng, Q. J. He, Z. W. Cui, K. L. Zhao, S. J. Zhang and J. L. Shi, *Chem. Sci.*, 2015, **6**, 1747-1753.
9. Z. Sheng, D. Hu, M. Zheng, P. Zhao, H. Liu, D. Gao, P. Gong, G. Gao, P. Zhang, Y. Ma and L. Cai, *ACS nano*, 2014, **8**, 12310-12322.
10. C. Li, T. Chen, I. Ocsoy, G. Zhu, E. Yasun, M. You, C. Wu, J. Zheng, E. Song, C. Z. Huang and W. Tan, *Adv. Funct. Mater.*, 2014, **24**, 1772-1780.
11. H. Deng, Y. Zhong, M. Du, Q. Liu, Z. Fan, F. Dai and X. Zhang, *Theranostics*, 2014, **4**, 904-918.
12. J. Peng, T. Qi, J. Liao, B. Chu, Q. Yang, Y. Qu, W. Li, H. Li, F. Luo and Z. Qian, *Theranostics*, 2014, **4**, 678-692.
13. H. Xing, X. Zheng, Q. Ren, W. Bu, W. Ge, Q. Xiao, S. Zhang, C. Wei, H. Qu, Z. Wang, Y. Hua, L. Zhou, W. Peng, K. Zhao and J. Shi, *Sci. Rep.*, 2013, **3**, 1751.
14. H. Ke, J. Wang, S. Tong, Y. Jin, S. Wang, E. Qu, G. Bao and Z. Dai, *Theranostics*, 2013, **4**, 12-23.
15. L. Zhang, S. Gao, F. Zhang, K. Yang, Q. Ma and L. Zhu, *ACS nano*, 2014, **8**, 12250-12258.
16. S. Bhuniya, S. Maiti, E. J. Kim, H. Lee, J. L. Sessler, K. S. Hong and J. S. Kim, *Angew. Chem. Int. Ed. Engl.*, 2014, **53**, 4469-4474.
17. J. Shi, T. W. Liu, J. Chen, D. Green, D. Jaffray, B. C. Wilson, F. Wang and G. Zheng, *Theranostics*, 2011, **1**, 363-370.
18. R. R. Ye, C. P. Tan, L. He, M. H. Chen, L. N. Ji and Z. W. Mao, *Chem. Commun.*, 2014, **50**, 10945-10948.
19. Vı ´ctor M. Jime´nez-Pe´rez, Marı ´a C. Garcı ´a-Lo´pez, Blanca M. Mun˜oz-Flores, Rodrigo Chan-Navarro, Jessica C. Berrones-Reyes, H. V. Rasika Dias, Ivana Moggio, Eduardo Arias, J. s. A. Serrano-Mireles and A. Chavez-Reyes, *J. Mater. Chem. B*, 2015, DOI: 10.1039/c5tb00717h.
20. W. Fan, B. Shen, W. Bu, F. Chen, K. Zhao, S. Zhang, L. Zhou, W. Peng, Q. Xiao, H. Xing, J. Liu, D. Ni, Q. He and J. Shi, *J. Am. Chem. Soc.*, 2013, **135**, 6494-6503.
21. Q. Xiao, X. Zheng, W. Bu, W. Ge, S. Zhang, F. Chen, H. Xing, Q. Ren, W. Fan, K. Zhao, Y. Hua and J. Shi, *J. Am. Chem. Soc.*, 2013, **135**, 13041-13048.
22. A. Al Zaki, D. Joh, Z. Cheng, A. L. De Barros, G. Kao, J. Dorsey and A. Tsourkas, *ACS nano*, 2014, **8**, 104-112.
23. J. Buentzel, O. Micke, K. Kisters, F. Bruns, M. Glatzel, K. Schoenekaes, G. Kundt, U. Schaefer and R. Muecke, *Anticancer Res.*, 2010, **30**, 1783-1786.
24. I. M. Puspitasari, R. Abdulah, C. Yamazaki, S. Kameo, T. Nakano and H. Koyama, *Radiat. Oncol.*, 2014, **9**, 125.
25. Y. Huang, L. He, W. Liu, C. Fan, W. Zheng, Y. S. Wong and T. Chen, *Biomaterials*, 2013, **34**, 7106-7116.
26. W. Liu, X. Li, Y. S. Wong, W. Zheng, Y. Zhang, W. Cao and T. Chen, *ACS nano*, 2012, **6**, 6578-6591.
27. H. L. Wu, X. L. Li, W. Liu, T. F. Chen, Y. H. Li, W. J. Zheng, C. W. Y. Man, M. K. Wong and K. H. Wong, *J. Mater. Chem.*, 2012, **22**, 9602-9610.
28. T. Chen and Y. S. Wong, *Cell Mol. Life Sci.*, 2008, **65**, 2763-2775.
29. T. Chen and Y. S. Wong, *Int. J. Biochem. Cell B.*, 2009, **41**, 666-676.
30. Y. H. Li, X. L. Li, W. J. Zheng, C. D. Fan, Y. B. Zhang and T. F. Chen, *J. Mater. Chem. B*, 2013, **1**, 6365-6372.
31. B. Yu, H. Li, J. H. Zhang, W. J. Zheng and T. F. Chen, *J. Mater. Chem. B*, 2015, **3**, 2497-2504.
32. F. Yang, Q. Tang, X. Zhong, Y. Bai, T. Chen, Y. Zhang, Y. Li and W. Zheng, *Int. J. Nnanomed.*, 2012, **7**, 835-844.
33. Y. Liu, Y. Luo, X. Li, W. Zheng and T. Chen, *Chem-Asian J*, 2015, **10**, 642-652.
34. M. Zhou, S. Ji, Z. Wu, Y. Li, W. Zheng, H. Zhou and T. Chen, *Eur. J. Med. Chem.*, 2015, **96**, 92-97.
35. Y. W. Liang, J. Zheng, X. Li, W. Zheng and T. Chen, *Eur. J. Med. Chem.*, 2014, **84**, 335-342.
36. D. Plano, E. Moreno, M. Font, I. Encio, J. A. Palop and C. Sanmartin, *Arch. Pharm.*, 2010, **343**, 680-691.
37. W. Wang, L. Li, S. Liu, C. Ma and S. Zhang, *J. Am. Chem. Soc.*, 2008, **130**, 10846-10847.
38. J. Kochansky, C. Cohen, W. Lusby, J. Svoboda, J. Feldmesser and F. Wright, *J. Agr. Entomol.*, 1988.
39. Q. Xie, Y. Zhou, G. Lan, L. Yang, W. Zheng, Y. Liang and T. Chen, *Biochem. Bioph. Res. Co.*, 2014, **449**, 88-93.
40. Q. Xie, L. Z. He, H. Q. Lai, W. J. Zheng and T. F. Chen, *Rsc. Adv.*, 2014, **4**, 34210-34216.
41. W. Dorr, *Strahlenther. Onkol.*, 2006, **182**, 693-695.
42. S. Urig and K. Becker, *Semin. Cancer Biol.*, 2006, **16**, 452-465.
43. J. Lu and A. Holmgren, *Free Radical Bio. Med.*, 2014, **66**, 75-87.
44. S. Gromer, S. Urig and K. Becker, *Med. Res. Rev.*, 2004, **24**, 40-89.
45. C. Fan, J. Chen, Y. Wang, Y. S. Wong, Y. Zhang, W. Zheng, W. Cao and T. Chen, *Free Radical Bio. Med.*, 2013, **65**, 305-316.
46. C. Fan, W. Zheng, X. Fu, X. Li, Y. S. Wong and T. Chen, *Cell Death Dis.*, 2014, **5**, e1191.
47. R. Rubbiani, I. Kitanovic, H. Alborzinia, S. Can, A. Kitanovic, L. A. Onambele, M. Stefanopoulou, Y. Geldmacher, W. S. Sheldrick, G. Wolber, A. Prokop, S. Wolfl and I. Ott, *J. Med. Chem.*,2010, **53**, 8608-8618.
48. R. W. Y. Sun, C. N. Lok, T. T. H. Fong, C. K. L. Li, Z. F. Yang, T. T. Zou, A. F. M. Siu and C. M. Che, *Chem. Sci.*, 2013, **4**, 1979-1988.
49. T. Zou, C. T. Lum, C. N. Lok, W. P. To, K. H. Low and C. M. Che, *Angew. Chem. Int. Ed. Engl.*, 2014, **53**, 5810-5814.
50. I. L. Martins, C. Charneira, V. Gandin, J. L. Ferreira da Silva, G. C. Justino, J. P. Telo, A. J. Vieira, C. Marzano and A. M. Antunes, *J. Med. Chem.*, 2015, **58**, 4250-4265.
51. B. Zhang, D. Duan, C. Ge, J. Yao, Y. Liu, X. Li and J. Fang, *J. Med. Chem.*, 2015, **58**, 1795-1805.
52. J. Yan, Y. Guo, Y. Wang, F. Mao, L. Huang and X. Li, *Eur. J. Med. Chem.*, 2015, **95**, 220-229.
53. T. Chen, W. Zheng, Y. S. Wong and F. Yang, *Biomed. Pharmacother.*, 2008, **62**, 77-84.
54. C. Liu, Z. Liu, M. Li, X. Li, Y. S. Wong, S. M. Ngai, W. Zheng, Y. Zhang and T. Chen, *PloS one*, 2013, **8**, e53945.
55. A. Meyer, C. P. Bagowski, M. Kokoschka, M. Stefanopoulou, H. Alborzinia, S. Can, D. H. Vlecken, W. S. Sheldrick, S. Wolfl and I. Ott, *Angew. Chem. Int. Ed. Engl.*, 2012, **51**, 8895-8899.
56. M. H. Lee, J. H. Han, J. H. Lee, H. G. Choi, C. Kang and J. S. Kim, *J. Am. Chem. So.*, 2012, **134**, 17314-17319.
57. V. Pierroz, T. Joshi, A. Leonidova, C. Mari, J. Schur, I. Ott, L. Spiccia, S. Ferrari and G. Gasser, *J. Am. Chem. So.*, 2012, **134**, 20376-20387.
58. X. L. Li, T. Chen, Y. S. Wong, G. Xu, R. R. Fan, H. L. Zhao and J. C. Chan, *Int. J Biochem. Cell B.*, 2011, **43**, 525-534.
59. Y. Li, X. Li, Y. S. Wong, T. Chen, H. Zhang, C. Liu and W. Zheng, *Biomaterials*, 2011, **32**, 9068-9076.
60. T. Chen and Y. S. Wong, *J. Agr. Food Chem.*, 2008, **56**, 10574-10581.
61. L. Li, W. Cao, W. Zheng, C. Fan and T. Chen, *Dalton T.*, 2012, **41**, 12766-12772.
62. L. He, H. Lai and T. Chen, *Biomaterials*, 2015, **51**, 30-42.
63. T. Chen, Y. S. Wong, W. Zheng, Y. Bai and L. Huang, *Colloid. Surf. B.*, 2008, **67**, 26-31.

View Article Online
DOI: 10.1039/C5TB01501D

TABLE OF CONTENT

Herein we have identified selenadiazole derivatives as effective and safe theranostic agents for simultaneous cancer chemo-/radiotherapy.